

Noise Resistant Phase Imaging with Intensity Correlation

Jerzy Szuniewicz¹, Stanisław Kurdziałek¹, Sanjukta Kundu¹, Wojciech Zvolinski¹,
Radosław Chrapkiewicz², Mayukh Lahiri³, Radek Lapkiewicz^{1*}

¹Institute of Experimental Physics, Faculty of Physics, University of Warsaw,
ul. Pasteura 5, 02-093 Warszawa, Poland,

²CNC Program, Stanford University, Palo Alto, CA 94304, United States

³Oklahoma State University, Stillwater, OK 74078-3072, United States

*radek.lapkiewicz@fuw.edu.pl

Interferometric methods, renowned for their reliability and precision, play a vital role in phase imaging. Interferometry typically requires high coherence and stability between the measured and the reference beam. The presence of rapid phase fluctuations averages out the interferogram, erasing the spatial phase information. This difficulty can be circumvented by shortening the measurement time. However, shortening the measurement time results in smaller photon counting rates precluding its applicability to low-intensity phase imaging. We introduce and experimentally demonstrate a phase imaging technique that is immune to position-independent, time-dependent phase fluctuation. We accomplish this by measuring intensity correlation instead of intensity. Our method enables using long measurement times and is therefore advantageous when the photon flux is very low. We use a Fisher information-based approach to show that the precision of phase reconstruction achieved using our method is in fact the best achievable precision in the scenario when two photons are detected per phase stability time.

Introduction

Phase imaging is important for applications spanning many diverse fields, including biological imaging (1), and phase microscopy (2, 3). Measurements of the phase shifts within samples can yield information about the refractive index, thickness, and structure of an object. Interferometry (4) is a very powerful tool that is often used in phase imaging of an object (5). Interferometric measurements allow the detection of small variations in optical paths. There are numerous interferometric techniques such as the ones regularly used in optical coherence tomography (6, 7) or quantitative phase microscopy (8). Some of the techniques, especially those related to biology, require very low photon fluxes. For an interferometric measurement a wave field that has interacted with an object is superposed with a reference field and the resulting interference pattern is detected by a camera. If the object field (probe field) and the reference

field are mutually coherent, the time-averaged intensity on camera is given by (9, 10):

$$I(x, y) = I_r + I_o + 2\sqrt{I_r I_o} \cos[\phi_{in} + \phi(x, y)], \quad (1)$$

where I_r and I_o are the averaged intensity of the reference and the object fields, respectively, ϕ_{in} is the interferometric phase that can be changed by introducing spatial or temporal delays between the two fields, and $\phi(x, y)$ is the phase map of the object. Standard interferometric phase imaging techniques are based on the signature of $\phi(x, y)$ left in the detected intensity pattern. However, for any such method to be applicable, the object field and the reference field need to be mutually coherent. Time-dependent, uncontrollable phase fluctuations introduce incoherence between object and reference fields. The method is therefore vulnerable to time-dependent, uncontrollable phase fluctuations that introduce incoherence between object and reference fields.

When the phase fluctuates much faster compared to the detection time, the coherence between the object and image fields is practically lost and, no interference will be observed, i.e.,

$$I(x, y) = I_r + I_o. \quad (2)$$

Since there is no information of $\phi(x, y)$ in this intensity pattern, the standard phase imaging scheme becomes inapplicable to this case. One way to avoid the effect of this time-dependent phase fluctuation is to shorten the duration of measurement (11). A short measurement time, however, reduces the amount of detected light and is therefore impractical for imaging photo-sensitive biological specimens, which require low-intensity light. Furthermore, for interferometric fluorescence super-resolution microscopy (12), often very low-intensity light (13) needs to be superposed. In such cases, any time-dependent phase fluctuations must be avoided due to the relatively long detection time requirement.

Here, we introduce a method of phase imaging that is fully resistant to time-dependent phase fluctuations as long as it is possible to measure at least two photons per phase stability time. Our method is fundamentally different from the standard phase imaging techniques (14), as we do not need interferometric phase stability due to the fact that we measure intensity correlation instead of intensity.

The scheme of our experiment is illustrated in Fig. 1. A wave field that has interacted with an object (object field) is superposed with a reference field and the resulting interference pattern is detected by a camera. A time-dependent phase fluctuation $\Theta(t)$ is introduced in the reference field. Under these circumstances, no information on $\phi(x, y)$ can be retrieved from the intensity pattern given by Eq. (2), and therefore the standard phase imaging techniques become inapplicable. In the present article, we introduce a method of phase imaging that is resistant to time-dependent phase fluctuations, provided that phase change is uniform throughout the entire sample (15). Our method relies on measuring intensity correlations of light and is inspired by the intensity interferometry technique introduced by Hanbury Brown and Twiss (HBT) (16). The HBT method and its generalizations were applied to a variety of light sources (17–25) and similarly our technique might be applied in various scenarios including laser and thermal light as important examples.

We determine the correlation function between the intensities measured at a pair of points (x, y) and (x', y')

$$\langle \tilde{I}(x, y; t) \tilde{I}(x', y'; t) \rangle \propto 1 \pm \frac{1}{2} \cos [\phi(x, y) - \phi(x', y')], \quad (3)$$

where $\tilde{I}(x, y; t)$ is the instantaneous intensity measured at a point (x, y) at time t . On the right hand side

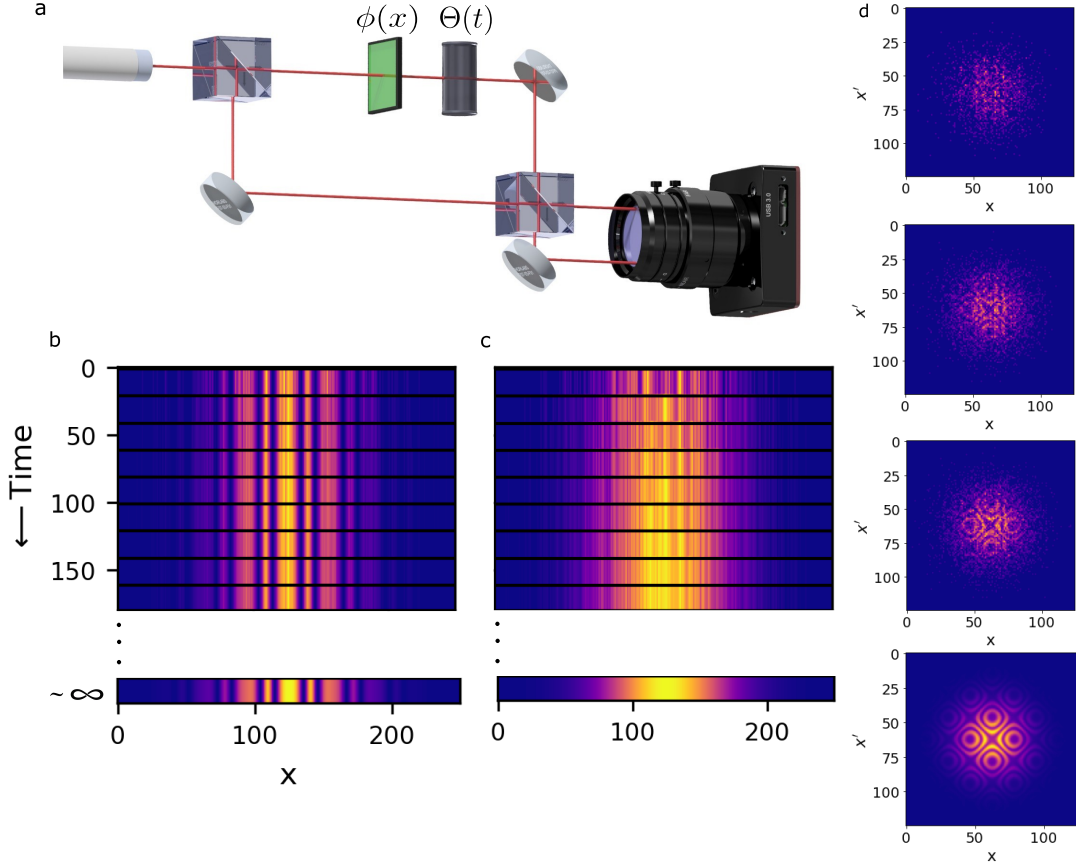


Figure 1: **(a)** Simplified schematic of the experiment: we divide input light into two paths, an object path($\phi(x)$), and a reference path. In the object path, we introduce a spatially varying phase that we want to image. A time-fluctuating interferometric phase can be introduced to the system ($\Theta(t)$) with no loss in the quality of the phase retrieval. For slowly fluctuating phase $\Theta(t)$, we can measure high visibility interference fringes **(b)**, but no interferogram can be recorded due to insufficient photon statistics and rapid fluctuations of ($\Theta(t)$) - depicted in the image **(c)** - where fringes average to the intensity profile of the beam having no phase information. Images **(b)** and **(c)** depict normalized one photon interference fringes for slowly and highly fluctuating cases respectively. We also depict second-order correlation interferograms **(d)** for the same photons constituting the interferograms in image (c). Even for this highly fluctuating case, where we record only a few photons within the stability time of the phase $\Theta(t)$, we can retrieve high visibility second-order correlation interferograms preserving full phase information about the measured phase $\phi(x)$.

of Eq. (3), the plus (+) and minus (-) signs apply when the two points of measurement are in the same and different beam splitter outputs, respectively. We also assume, $I_r = I_o$. Note that the information about the phase map of the object, which was lost in the intensity pattern [Eq. (2)], reappears in the intensity correlation [Eq. (3)].

The 2nd-order intensity correlations map contains the full information required to optimally reconstruct $\phi(x, y)$ in the extreme case when only two photons are detected during the phase stability time. Our strategy of reconstructing the actual phase distribution in this scenario is optimal, which we prove rigorously using estimation theory tools, namely Fisher Information and Cramér-Rao bound (see Supplementary S_1 for detail).

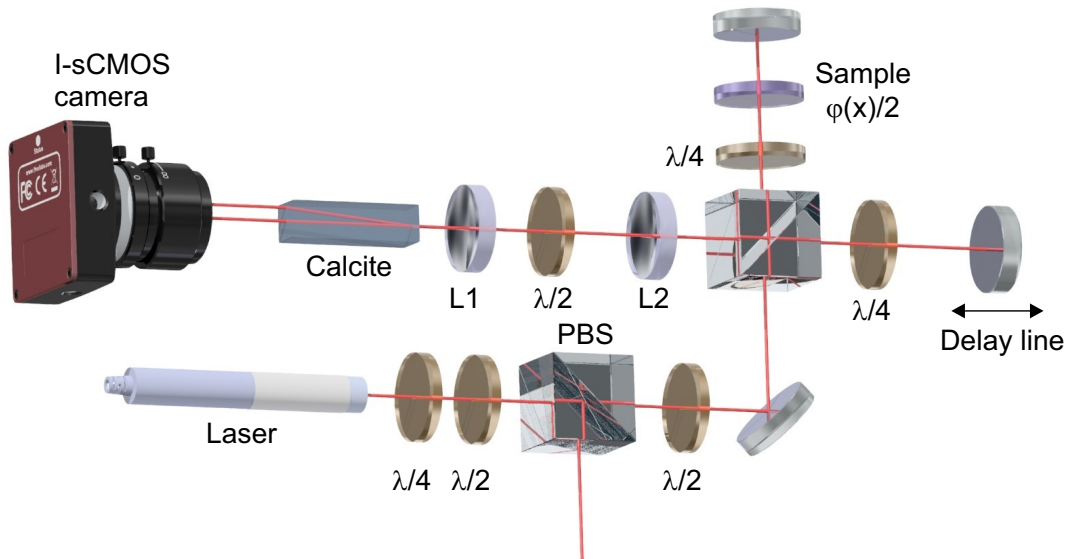


Figure 2: Experimental setup for noise-resistant phase imaging. The incoming beam of Laser after passing through a $\frac{\lambda}{2}$ - half-wave plate, $\frac{\lambda}{4}$ - quarter wave plate, PBS - polarization beam splitter, and another $\frac{\lambda}{2}$ plate, the beam enters a Michelson type interferometer. Each of the two paths in the interferometer is encoded with orthogonal polarization. In one arm the spatial phase $\phi(x)$ is introduced next to the surface of the interferometer mirror. The interferometric mirror in the other arm is given a phase fluctuation by attaching it to a piezoelectric actuator. The two beams of the interferometric arms after combining at the PBS pass through L1, and L2 lenses. The calcite polarizer acts as a 50/50 Beamsplitter. The I-sCMOS - Intensified sCMOS camera records single photons at both outputs of the interferometer. The use of short exposure time of the I-sCMOS, in the single nanosecond timescale, gives it stability and resistance against fluctuations up to tens of MHz.

Experimental setup

The experimental setup is depicted in Fig.2. Light from a polarized, coherent source (780 nm laser) is attenuated, spatially filtered, and directed to two arms of a polarization-based Michelson interferometer. In order to prepare the object beam, in one of the arms, we place a phase mask to imprint spatially varying phase $\phi(x)$ to the beam. We perform experiments with three kinds of different phase masks applied to our object beam. We imprint a 1D quadratic local phase profile to the beam by placing a cylindrical lens of focal length, $f = 1000$ mm in proximity to the mirror (Fig. 2). Additionally, we also use a spatial light modulator (SLM) as a phase mask, as it can display any arbitrary phase profile. We imprint 1D

exponential and sinusoidal phases to our object beam by the SLM display (see supplementary S_2 for detail).

A time-dependent phase fluctuation is introduced in the other arm (the reference beam) to make it incoherent with the object beam. This is realized with a piezoelectric actuator driven by a RAMP. Light is combined on the PBS. Object and the reference planes are imaged onto two regions of an Intensified sCMOS (I-sCMOS) (26) camera with a 4f system using lenses L_1 and L_2 . After the PBS, the object and the reference beams are distinguishable due to their orthogonal polarization. In order to observe interference we rotate their polarization by 45 degrees with a half-wave plate and we perform the projective measurement in the original bases with a calcite crystal. This mixes the light from both outputs and allows us to observe interference in both outputs of the beam splitter. The visibility is reduced due to imperfect imaging because of the path length difference in the calcite. In order to register very low photon flux and to minimize exposure time to circumvent fluctuations, we use an Intensified-sCMOS camera. We collect the data with a frame rate of 200 Hz. choosing a low exposure time $T_{\text{exp}} \sim ns$ allows performing measurement under phase fluctuations with frequency up to ($f_n \sim 1/T_{\text{exp}}$) tens of MHz.

Results

Data measured in our experiment consist of an average of 15 photons at both outputs of the interferometer per frame. We remove temporal correlations between subsequent frames by randomly permuting the order of frames before further processing—this process does not change the performance of our method but allows us to simulate the conditions, in which the global phase fluctuates faster than the camera frame rate. In such conditions, it is impossible to retrieve phases using standard interferometric methods. Averaging recorded intensities over multiple frames or increasing measurement time would result in a loss of the visibility of the interference fringes. In contrast, we average correlations of detected photons’ positions without any loss of the phase information. Such averaging over multiple frames results in the reproduction of the correlation function (Eq.3), from which we can retrieve the phase profile using the standard digital holography method, Fourier off-axis holography (27). The correlation function is measured from the coincidence map of the detected photons’ positions. This analyzing mechanism is the essence of our noise-resistant phase imaging technique. 1D quadratic phase measurement introduced by the cylindrical lens is shown in Fig. 3. The measured coincidence map (Fig. 3(a)) consists of approximately 10^7 registered photon pairs with the mean number of coincidences per pixel as 100. We estimate the phase profile shape using the collected data, and compute the Mean Squared Error (MSE) between the measured and real value. As we show in Fig. 3(c), the MSE drops down with the total number of measured photons, and eventually reaches the theoretical minimum, obtained with the help of the Cramér-Rao bound (see Supplement 2 for details). This proves, that our method of phase estimation is optimal when at most two photons are measured during the phase stability time—notice, that this is the most extreme limit in which one can gain any information about the phase profile.

SLM-encoded phase measurements shown in Fig. 4(a), (b), and (c) represent the measured hologram, the retrieved phase, and the error per pixel respectively when the sinusoidal phase is applied. Similarly, Figs. 4(e), (f), and (g) represent the measured hologram, the retrieved phase, and the error per pixel respectively when the 1D exponential phase is applied. Errors in the retrieved respective phases (Fig. 4(c), Fig. 4(g)) are due to a finite number of pixels on the SLM and discrete values of the displayed phases.

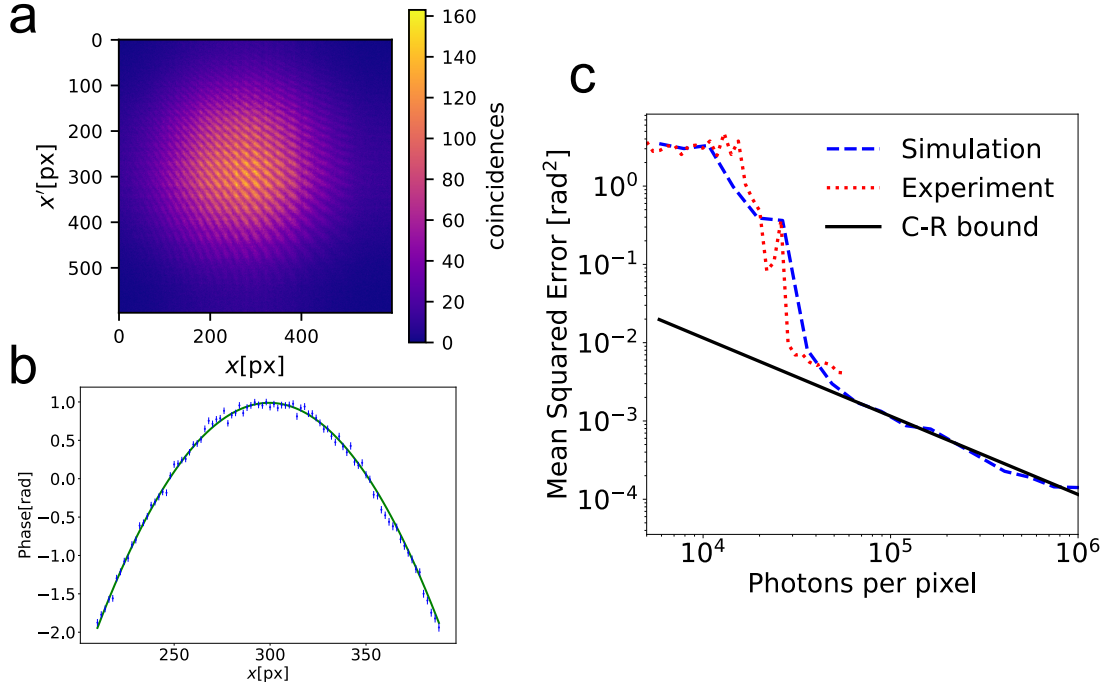


Figure 3: **(a)** represents the measured coincidence map for a 1D quadratic phase profile, plotted with a solid line in **(b)**. The reconstructed phase with error bars is also shown in **(b)**. The visibility of the fringes in the correlation map **(a)** is equal to $0.6^2/2$ (theoretical maximum with classical light is $1/2$). The total number of coincidences detected in the experiment is $\sim 10^7$. By randomly removing a part of the collected signal, we can check how the Mean Squared Error (MSE) associated with the phase reconstruction scales with the mean number of photons detected in one pixel during the whole experiment **(c)**. The MSE from the experiment is then compared with the MSE obtained using simulated hologram, with the same parameters as in the experiment. We calculate the fundamental Cramér-Rao (C-R) lower bound on the MSE, assuming the visibility of hologram fringes to be equal to $0.6^2/2$ (as in our experiment). When no noise apart from shot noise is present (as in simulation), our method allows to saturate this fundamental limit for large enough ($\sim 5 \cdot 10^4$) number of photons detected per pixel. Other possible sources of noise (e.g.) dark counts may slightly affect the MSE obtained experimentally.

Here we show that it is possible to retrieve complete phase profiles only with an average of two photons detected per frame which is an absolute minimum of detected photons per frame.

Conclusion and Discussion

In conclusion, we demonstrate a complete retrieval of phase patterns in the presence of high-frequency random phase fluctuations up to the order of tens of MHz when standard phase imaging techniques fail due to the scarcity of photons within a stable phase time interval. Our method is applicable to light sources described with different statistics, such as for example thermal light sources, and can be extended to interference between independent sources (21, 28).

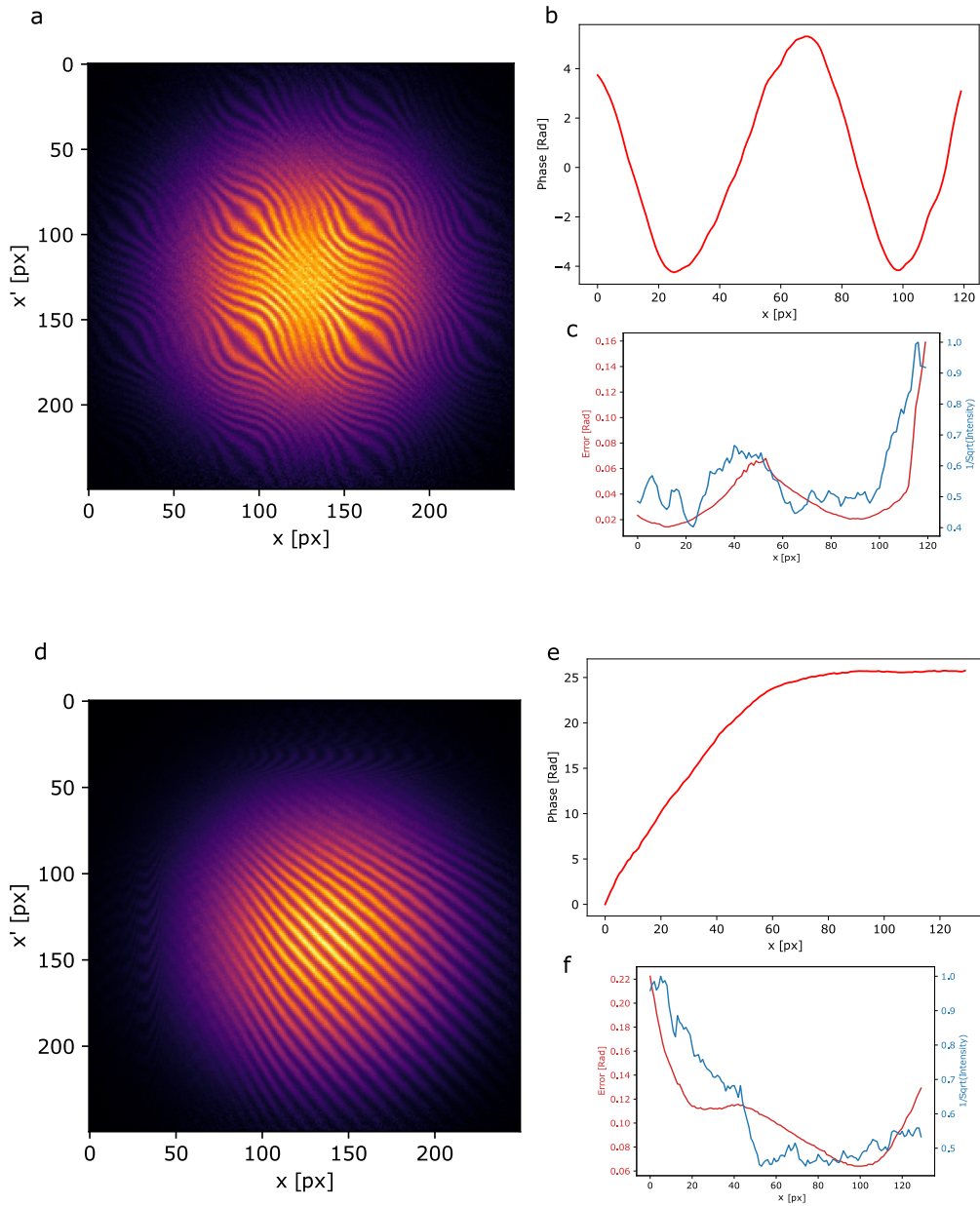


Figure 4: Experimental measurement of the spatial phases with the SLM - spatial light modulator. Measured coincidence maps (correlation functions) between outputs of the interferometer for **(a)** sinusoidal, and **(d)** exponential phases set on SLM. Each axis of coincidence maps represents the positions of photons detected along one output of the interferometer. **(b)** and **(e)** represent the aforementioned reconstructed phases. **(c)** and **(f)** show errors and square-root of the intensities.

We want to highlight, that the presented method optimality is proven using the Cramer-Rao bound – all the spatial phase information stored in the detected photons is retrieved (29).

High temporal resolution (short gating time) is necessary for overcoming the problem of the rapidly fluctuating temporal phases. Such high temporal resolution in our experiment was obtained using an image-intensified camera, which allows us to collect data with short exposure times down to a few nanoseconds. However, our method is not limited to this camera type and can be implemented using various high-temporal resolution detection platforms. Because of high quantum efficiency, temporal resolution, and low noise level in recent single-photon avalanche diode (SPAD) array technology (30) development, our method can also be implemented by SPAD arrays in the future. We stress that the technique can be implemented both in the photon counting regime and by employing less accurate intensity measurements, yet it is the most remarkable for cases where registering more than two photons per phase stability time is rare. Our method can be readily generalized to two-dimensional spatial phase profiles by creating higher-dimensional correlation maps. It also allows for implementation in different degrees of freedom, such as temporal or spectral, allowing the creation of joint probability maps both for photon detection times or their detected wavelengths. It is also possible to incorporate an additional degree of freedom to a measurement, measuring for instance joint temporal-spatial correlations maps.

Additionally, this method could be expanded for different situations, in which multiple photons are detected or photons are registered at the same output. Each pair of photons can be treated as a separate coincidence, so the number of coincidences scales with a number of detected photons n as $\binom{n}{2}$. We can also create such coincidence maps for multiple photons within each of the interferometer outputs as well as between them. Such holograms can build up much faster and shorten measurement time while the physics behind them is the same.

This method is only valid when all values of the global phase Θ have the same probability of appearing during the time interval in which the whole measurement is performed. To satisfy this condition for arbitrary temporal phase noise, it is enough to add random uniformly distributed signal oscillating between 0 and 2π to the unknown global phase fluctuations $\Theta(t)$. In fact, the added noise can be much slower than the rate of phase global phase fluctuations $\Theta(t)$.

Our method opens up possible applications in wavefront sensing under low light conditions for microscopy as well as fundamental research. Unbalanced interferometers, such as ones used in the time-bin encoding could be of particular interest, as our method enables using additional degrees of freedom (multi-dimensional information encoding) while filtering out phase fluctuations arising, for instance, from unmatched optical paths. In addition, because of the shorter wavelengths of X-rays (also of neutrons or electrons), X-ray interferometry (31, 32) requires much tighter alignment and better mechanical stability of the interferometer. We emphasize that because our technique is phase noise resistant, it holds a potential for phase-sensitive imaging using X-ray interferometry. In addition, analogous techniques might also find applications in matter-wave interferometry (33, 34).

Acknowledgments

We acknowledge discussions with Piotr Wegrzyn, Lukasz Zinkiewicz, Michal Jachura, Wojciech Wasilewski, and Marek Zukowski. This work was supported by the Foundation for Polish Science under the FIRST TEAM project 'Spatiotemporal photon correlation measurements for quantum metrology and super-resolution microscopy' co-financed by the European Union under the European Regional Development

Fund (POIR.04.04.00-00-3004/17-00), and by the National Laboratory for Photonics and Quantum Technologies—NLPQT (POIR.04.02.00.00-B003/18).

Supplementary materials

S_1 - Fundamental precision limits of phase imaging with fluctuating reference arm

S_2 - Experimental setup details

References

1. Y. Park, C. Depeursinge, G. Popescu, *Nature Photonics* **12**, 578 (2018).
2. G. Popescu, T. Ikeda, R. R. Dasari, M. S. Feld, *Optics Letters* **31**, 775 (2006).
3. Z. Wang, *et al.*, *Optics Express* **19**, 1016 (2011).
4. P. Hariharan, Ed. 2, *Optical Interferometry* (Academic Press, 2003).
5. T. Ikeda, G. Popescu, R. R. Dasari, M. S. Feld, *Optics Letters* **30**, 1165 (2005).
6. D. Huang, *et al.*, *Science* **254**, 1178 (1991).
7. M. Sticker, C. K. Hitzenberger, R. Leitgeb, A. F. Fercher, *Optics Letters* **26**, 518 (2001).
8. E. Cuche, F. Bevilacqua, C. Depeursinge, *Optics Letters* **24**, 291 (1999).
9. E. Hecht, Ed. 5, Chapter 9, *Optics* (Pearson Education Limited, 2017).
10. G. Popescu, *Quantitative Phase Imaging of Cells and Tissues* (McGraw-Hill, New York, 2011).
11. G. Magyar, L. Mandel, *Nature* **198**, 255 (1963).
12. L. A. Rozema, *et al.*, *Phys. Rev. Lett.* **112**, 223602 (2014).
13. P. A. Morris, R. S. Aspden, J. E. C. Bell, R. W. Boyd, M. J. Padgett, *Nature Communications* **6** (2015).
14. R. J. Collier, C. B. Burckhardt, L. H. Lin, *Optical Holography* (Academic, 1971).
15. J. Szuniewicz, *et al.*, *Rochester Conference on Coherence and Quantum Optics (CQO-11)* (OSA, 2019).
16. R. Hanbury Brown, R. Q. Twiss, *Nature* **177**, 27 (1956).
17. C. K. Hong, Z. Y. Ou, L. Mandel, *Physical Review Letters* **59**, 2044 (1987).
18. Z. Y. Ou, E. C. Gage, B. E. Magill, L. Mandel, *Journal of the Optical Society of America B* **6**, 100 (1989).

19. T. B. Pittman, J. D. Franson, *Physical Review Letters* **90** (2003).
20. R. L. Pfleeger, L. Mandel, *Physical Review* **159**, 1084 (1967).
21. J. G. Rarity, P. R. Tapster, R. Loudon, *Journal of Optics B: Quantum and Semiclassical Optics* **7**, S171 (2005).
22. X. Li, L. Yang, L. Cui, Z. Y. Ou, D. Yu, *Optics Express* **16**, 12505 (2008).
23. A. J. Bennett, R. B. Patel, C. A. Nicoll, D. A. Ritchie, A. J. Shields, *Nature Physics* **5**, 715 (2009).
24. Y.-S. Kim, O. Slattery, P. S. Kuo, X. Tang, *Physical Review A* **87** (2013).
25. R. Chrapkiewicz, M. Jachura, K. Banaszek, W. Wasilewski, *Nature Photonics* **10**, 576 (2016).
26. R. Chrapkiewicz, W. Wasilewski, K. Banaszek, *Optics Letters* **39**, 5090 (2014).
27. J. Mertz, *Introduction to Optical Microscopy* (Roberts and Company Publishers, 2009.).
28. H. Paul, *Rev. Mod. Phys.* **58**, 209 (1986).
29. H. Cramér, *Mathematical methods of statistics*, vol. 26 (Princeton university press, 1999).
30. I. M. Antolovic, C. Bruschini, E. Charbon, *Optics Express* **26**, 22234 (2018).
31. I. Zanette, T. Weitkamp, T. Donath, S. Rutishauser, C. David, *Physical Review Letters* **105** (2010).
32. T. Weitkamp, B. Nöhammer, A. Diaz, C. David, E. Ziegler, *Applied Physics Letters* **86**, 054101 (2005).
33. E. M. Rasel, M. K. Oberthaler, H. Batelaan, J. Schmiedmayer, A. Zeilinger, *Physical Review Letters* **75**, 2633 (1995).
34. M. Arndt, A. Ekers, W. von Klitzing, H. Ulbricht, *New Journal of Physics* **14**, 125006 (2012).

Supplementary materials and methods

1 S1: Fundamental precision limits of phase imaging with fluctuating reference arm

1.1 The measurement model

Two cameras are set on the two outputs of the interferometer, each of them consists of the same number of pixels n_{pix} . The sample area giving the additional phase ϕ_i is imaged to the pixel number i on both cameras. Only two photons are received per the stability time of the interferometer phase. A single measurement consists of a detection of these two photons. The output of the single measurement is a pair $(i_{+/-}, j_{+/-})$. Numbers i, j stand for the numbers of pixels in which photons were detected, whereas indices $+$ or $-$ indicates in which of the two outputs the corresponding photon was measured. The probability of measuring a single photon in a pixel $i_{+/-}$ is:

$$p(i_{+/-}) = \tilde{N} I_i \frac{1}{2} (1 \pm v \cos(\phi_i + \theta)), \quad (1)$$

where \tilde{N} is a normalization factor, v is interferometer visibility, θ is an extra, global, fluctuating phase, and I_i is the intensity of the illuminating the phase mask in the area corresponding to pixel i . Phase θ is stable during the detection of each photon pair, its value for each pair is independently drawn from the continuous uniform probability distribution $U(0, 2\pi)$. There is no information about θ value in each experiment, so the observed probability of obtaining pair $(i_{+/-}, j_{+/-})$ in every single frame is:

$$p(i_{+/-}, j_{+/-}) = \int_0^{2\pi} p(i_{+/-}, j_{+/-}, \theta) d\theta \quad (2)$$

$p(i_{+/-}, j_{+/-}, \theta)$ is a joint probability distribution of measuring pair $(i_{+/-}, j_{+/-})$ with the fixed value of θ . From equation 2 we obtain the formulas:

$$p(i_+, j_+) = p(i_-, j_-) = N I_i I_j (2 + v^2 \cos(\phi_i - \phi_j)) \quad (3)$$

$$p(i_+, j_-) = p(i_-, j_+) = N I_i I_j (2 - v^2 \cos(\phi_i - \phi_j)) \quad (4)$$

N is a new normalization factor. The above equations are our starting point to further inference about the maximal precision of the measurement. Full information about each single measurement is included in the dependence of the probability p of the specific result of a measurement (i_{\pm}, j_{\pm}) on the estimated parameters ϕ_i .

1.2 Cramér-Rao bound

In order to calculate maximal precision of estimation of the parameters ϕ_i , Fisher Information (FI) matrix will be calculated. There are 4 different types of events, which can occur during one experiment - two photons may be detected in one output (+ or -) or in different outputs (we distinguish between +- and -+). We can distinguish between these 4 types, so the FI is the sum of FI matrices for all events' types:

$$F_{\text{tot}} = F_{++} + F_{--} + F_{+-} + F_{-+} \quad (5)$$

From equations 3 and 4 we can simply conclude, that $F_{++} = F_{--}$ and $F_{+-} = F_{-+}$. In the next part of the article F_{++} matrix will be calculated.

In order to simplify the formulas, the following notation will be used:

$$p(i_+, j_+) \equiv p(i, j), \quad \frac{\partial}{\partial \phi_k} \equiv \partial_k, \quad F \equiv F_{++}$$

The element of the FI matrix can be written in the following form:

$$F_{kl} = \sum_{i,j=1}^{n_{pix}} \frac{\partial_k p(i, j) \partial_l p(i, j)}{p(i, j)}, \quad (6)$$

Subsequently:

$$\partial_k p(i, j) = NI_i I_j v^2 (\delta_{jk} - \delta_{ik}) \sin(\phi_i - \phi_j) \quad (7)$$

$$\partial_k p(i, j) \partial_l p(i, j) = (\delta_{jk} - \delta_{ik})(\delta_{jl} - \delta_{il}) N^2 I_i^2 I_j^2 v^4 \sin^2(\phi_i - \phi_j) \quad (8)$$

Consequently, the matrix element is:

$$F_{kl} = \sum_{i,j=1}^{n_{pix}} \frac{(\delta_{jk} - \delta_{ik})(\delta_{jl} - \delta_{il}) NI_i I_j v^4 \sin^2(\phi_i - \phi_j)}{2 + v^2 \cos(\phi_i - \phi_j)} \quad (9)$$

If $k \neq l$, then for any m we have $\delta_{mk} \delta_{ml} = 0$, so $(\delta_{jk} - \delta_{ik})(\delta_{jl} - \delta_{il}) = -\delta_{jk} \delta_{il} - \delta_{ik} \delta_{jl}$. That means, that non-diagonal matrix elements are:

$$F_{kl} = -\frac{2NI_k I_l v^4 \sin^2(\phi_k - \phi_l)}{2 + v^2 \cos(\phi_k - \phi_l)}, \quad k \neq l \quad (10)$$

With the help of the equality $(\delta_{jk} - \delta_{ik})^2 = \delta_{jk} + \delta_{ik} - 2\delta_{ik} \delta_{jk}$ we can obtain diagonal terms of F :

$$F_{kk} = 2NI_k v^4 \sum_{i=1}^{n_{pix}} \frac{I_i \sin^2(\phi_i - \phi_k)}{2 + v^2 \cos(\phi_i - \phi_k)} \quad (11)$$

For any function f :

$$\sum_{i=1}^{n_{pix}} f(\phi_i, I_i) = n_{pix} \langle f(\phi_i, I_i) \rangle_i, \quad (12)$$

where $\langle f(\phi_i, I_i) \rangle_i$ is the mean value of the function over all pixels. In the next steps, the number of pixels is assumed to be big and each phase in the sample occurs with the same frequency. What is more, intensity of illuminating beam I_i is assumed to change slowly compared to the change of phase ϕ_i . In other words, many different phases occur in the region with approximately constant intensity. From these assumptions we obtain the equality:

$$\langle f(\phi_i, I_i) \rangle_i = \frac{1}{2\pi} \int_0^{2\pi} f(\phi, \langle I \rangle) d\phi, \quad (13)$$

where $\langle I \rangle$ stands for the mean intensity of the illuminating beam. Using the above assumptions, we can rewrite equation 11 as:

$$F_{kk} = 2NI_k \langle I \rangle v^4 \frac{n_{pix}}{2\pi} \int_0^{2\pi} \frac{\sin^2(\phi - \phi_k)}{2 + v^2 \cos(\phi - \phi_k)} d\phi \quad (14)$$

Consequently all diagonal terms of F are the same:

$$F_{kk} = 2N \langle I \rangle I_k n_{pix} (2 - \sqrt{4 - v^4}) \quad (15)$$

Now we need to calculate the value of a normalization factor N . We will use the fact, that sum of propabilities of all events must be equal to one:

$$\sum_{i,j=1}^{n_{pix}} p(i_+, j_+) + p(i_+, j_-) + p(i_-, j_+) + p(i_-, j_-) = 1 \quad (16)$$

Using equations 3 and 4 we obtain:

$$8N \sum_{i,j=1}^{n_{pix}} I_i I_j = 1 \quad (17)$$

We can rewrite the sum in the above equation as:

$$\sum_{i,j=1}^{n_{pix}} I_i I_j = \left(\sum_{i=1}^{n_{pix}} I_i \right)^2 = n_{pix}^2 \langle I \rangle^2 \quad (18)$$

and obtain:

$$N = \frac{1}{8n_{pix}^2 \langle I \rangle^2} \quad (19)$$

Finally F_{++} matrix can be written in the form:

$$F_{kl} = \begin{cases} \frac{1}{4n_{pix}} \frac{I_k}{\langle I \rangle} (2 - \sqrt{4 - v^4}) & \text{for } k = l \\ -\frac{1}{4n_{pix}^2} \frac{I_k I_l}{\langle I \rangle^2} \frac{2v^4 \sin^2(\phi_k - \phi_l)}{2 + v^2 \cos(\phi_k - \phi_l)} & \text{for } k \neq l \end{cases} \quad (20)$$

We have calculated F_{++} matrix, which is obviously similar to F_{--} matrix, because formulas for propabilities in both cases are the same. Analogous calculation show, that also $F_{+-} = F_{-+} = F_{++}$. Using the FI additivity we obtain the terms of F_{tot} matrix:

$$F_{\text{tot}} = 4F_{++} \quad (21)$$

This is the FI matrix for a single measurement. If the whole experiment consists of n_{mes} independent repetitions of the single measurement, we obtain the FI:

$$F_{\text{tot}}^{(n_{mes})} = 4n_{mes}F_{++} = 2n_{phot}F_{++}, \quad (22)$$

where n_{phot} stands for the total number of measured photons during the experiment. In the next part F stands for the whole FI associated with detection of n_{phot} number of photons. Terms of this matrix are:

$$F_{kl} = \begin{cases} \frac{n_{phot}}{n_{pix}} \frac{I_k}{\langle I \rangle} (1 - \sqrt{1 - v^4/4}) & \text{for } k = l \\ -\frac{n_{phot}}{2n_{pix}^2} \frac{I_k I_l}{\langle I \rangle^2} \frac{2v^4 \sin^2(\phi_k - \phi_l)}{2 + v^2 \cos(\phi_k - \phi_l)} & \text{for } k \neq l \end{cases} \quad (23)$$

From the Cramer-Rao bound, the minimal possible variance for estimating ϕ_k satisfy the inequality:

$$\Delta^2 \phi_k \geq (F^{-1})_{kk} \quad (24)$$

In general, the estimator which satisfy the above inequality may not exist, however, it is possible to get arbitrary close to the above bound if the number of measurement is big enough. That means, that the inequality becomes an equality if $n_{phot} \rightarrow \infty$. To simplify the calculations we also use the inequality:

$$(F^{-1})_{kk} \geq (F_{kk})^{-1}, \quad (25)$$

which is true for all hermitian F . It's clear, that in the general case the above inequality is not saturable. However, in our case the non-diagonal terms are asymptotically n_{pix} times smaller than diagonal terms. n_{pix} is also size of the F matrix. It may be proven, that for such scaling of non-diagonal terms with the size of matrix, the above inequality becomes saturable for $n_{pix} \rightarrow \infty$. Using both of above inequalities, we obtain the following bound:

$$\Delta \phi_k \geq \sqrt{\frac{n_{pix} \langle I \rangle}{n_{phot} I_k}} \frac{1}{\sqrt{1 - \sqrt{1 - v^4/4}}} \quad (26)$$

The value $n_k = \frac{n_{phot} I_k}{n_{pix} \langle I \rangle}$ may be interpreted as the expected value of photons detected in pixel number k (in any output). The above bound may be rewritten in the intuitive form:

$$\Delta \phi_k \geq \sqrt{\frac{1}{n_k}} \frac{1}{\sqrt{1 - \sqrt{1 - v^4/4}}} \quad (27)$$

From this form of the inequality it's clear, that the accuracy of measuring the value of the particular phase depends directly on the numer of photons interacting with the measured area.

1.3 Comparison with long-stability-time interferometer

Let's compare our result with the phase estimation precision limit for an interferometer with slowly fluctuating phase θ . First of all, let's notice that we can't beat the accuracy achievable in the situation, in which extra phase θ is known for all the detected photons. Indeed, the information we get in a situation with unknown θ is always smaller, even if the stability time if the interferometer is bigger. If θ values are known, each single photon detection could be treated as an independent event (which was not the case in the previous section). Let's calculate the FI matrix for the single photon detection when θ is fixed. Single measurement is fully described by the probability distribution from equation 1. Further we obtain:

$$\partial_k p(i_{+/-}) = \mp \frac{1}{2} \delta_{ki} \tilde{N} I_i v \sin(\phi_i + \theta) \quad (28)$$

In this case FI matrix has the form:

$$F_{kl} = \sum_{i=1}^{n_{pix}} \frac{\partial_k p(i_+) \partial_l p(i_+)}{p(i_+)} + \sum_{i=1}^{n_{pix}} \frac{\partial_k p(i_-) \partial_l p(i_-)}{p(i_-)} \quad (29)$$

From equation 28 it's clear, that all non-diagonal terms of the F matrix are equal to zero. This is because we obtain information about the ϕ_i phase only in case of detection a photon in the pixel $i_{+/-}$. The diagonal terms are:

$$F_{kk} = \tilde{N} I_i \frac{v^2 \sin^2(\phi_i + \theta)}{1 - v^2 \cos^2(\phi_i + \theta)} \quad (30)$$

To make this case similar to the case described in the previous section let's assume, that θ fluctuates and each value of θ appears with the same frequency (the difference is that θ fluctuates slowly and we know it's value). Then the mean FI for the single measurement is:

$$\langle F_{kk} \rangle_\theta = \frac{1}{2\pi} \int_0^{2\pi} F_{kk} d\theta = \frac{I_i}{n_{pix} \langle I \rangle} (1 - \sqrt{1 - v^2}), \quad (31)$$

where formula $\tilde{N} = \frac{1}{n_{pix} \langle I \rangle}$ obtained from the normalization condition was used. If n_{mes} measurements were made, n_{phot} photons were consumed. If we define $n_k = \frac{n_{phot} I_k}{n_{pix} \langle I \rangle}$ as in the previous section, we obtain the best possible accuracy of measuring each phase ϕ_k :

$$\Delta \phi_k \geq \sqrt{\frac{1}{n_k} \frac{1}{\sqrt{1 - \sqrt{1 - v^2}}}} \quad (32)$$

Equation 32 is very similar to the equation 27- the only difference is that term $\frac{v^4}{4}$ is substitute by the term v^2 . That means, that having only two photons per phase fluctuations stability time, leads to decrease of the effective visibility of the interferometer from v to $\frac{v^2}{2}$. As it was mentioned, it's not possible to beat the bound from equation 32 if θ value is not known in each measurement, even if the number of detected photons

in a phase stability time was increased. However, we can get close to that bound, if the phase stability time is big enough. Indeed, if we can measure many photons, when θ is stable, we don't really need to care about its unknown value and obtain **relative** values of ϕ_k using the same method as in case of known θ (it might be assumed to equal 0). This scheme is repeated independently for each θ . The bound from the equation 30 is saturated, because the number of measurements is big enough. That means, that we can also saturate the bound resulting from the mean FI (equation 32).

2 S2: Experimental setup details

This is a polarization-based Michelson interferometer. As a light source, we use a diode laser at a wavelength of 780 nm coupled to a single-mode fiber. At the output of the fiber, for polarization control, the attenuated beam passes through a half-wave plate, a quarter-wave plate, and polarizing beam splitter (PBS), and another half-wave plate, and then enters a Michelson-type interferometer. Each of the two paths in the interferometer is encoded with orthogonal polarization. In order to prepare the object beam, in one of the arms of the interferometer, we build two kinds of slightly modified setups - one with a cylindrical lens placed in front of one of the mirror in the horizontally polarized light beam path in the Michelson interferometer while in the other setup we replace the mirror in the same path with a spatial light modulator (SLM), thereby introducing spatially varying phase $\phi(x)$ onto the beam in that path. In one arm the spatial phase $\phi(x)$ is introduced next to the surface of the interferometer mirror. The interferometric mirror in the other arm is given a phase fluctuation by attaching it to a piezoelectric actuator.

We perform experiments with three kinds of different phase masks applied to our object beam. Our first configuration is to imprint a one dimensional quadratic local phase profile to the beam by placing a cylindrical lens of focal length, $f = 1000$ mm in proximity to the mirror (Fig. 2 in the main text). Additionally, in our second configuration with SLM (from the HOLOEYE PLUTO) as a phase mask, we can display any arbitrary phase profile. As an example, we imprint one dimensional exponential and sinusoidal phases to our object beam by the SLM display.

We introduce a time-dependent phase fluctuation in the other arm (the reference beam - vertically polarized beam path in the interferometer) to make it incoherent with the object beam. This is realized with a piezoelectric actuator driven by a RAMP of 1.234 Hz. This shouldn't be confused with the maximal noise frequency for which our method works. Both of the object and reference beams are combined on the polarizing beam splitter (PBS). Afterthat, they are imaged onto two regions of an Intensified sCMOS (I-sCMOS - with the image intensifier from Hamamatsu V7090D-71-G272 and sCMOS from Andor Zyla) camera with a 4f system using lenses L3 and L4 of focal length 200 mm. To observe the interference, the orthogonally polarized object and the reference beam are required to be indistinguishable, and to do so, we rotate the polarization of both beams by 45 degrees with a half-wave plate and we perform projective measurement in the original bases with a calcite crystal. Here, the calcite acts as a 50/50 Beamsplitter.

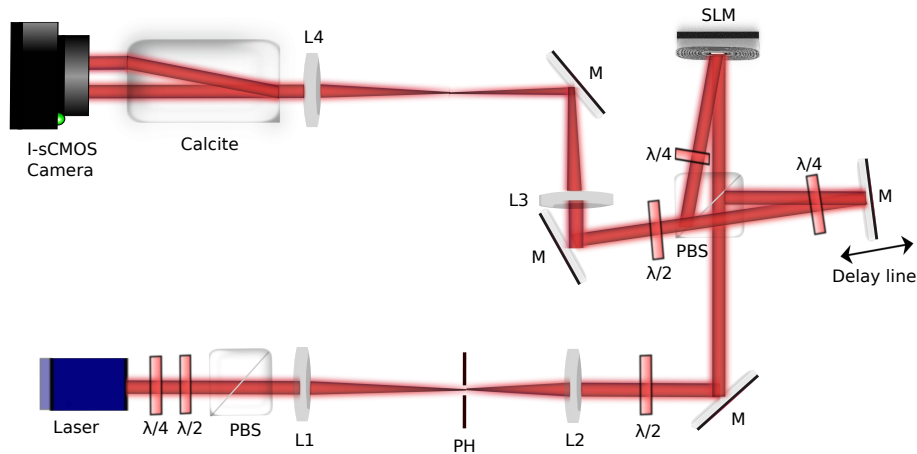


Figure 1: Experimental setup for noise-resistant phase imaging. The incoming beam of Laser after passing through a $\lambda/2$ - half-wave plate, $\lambda/4$ - quarter wave plate, PBS - polarization beam splitter, and another $\lambda/2$ plate, the beam enters a Michelson type interferometer. Each of the two paths in the interferometer is encoded with orthogonal polarization. In one arm the spatial phase $\phi(x)$ is introduced by the spatial light modulator (SLM). The interferometric mirror in the other arm is given a phase fluctuation by attaching it to a piezoelectric actuator. The two beams of the interferometric arms after combining at the PBS pass through L3, and L4 lenses. The calcite polarizer acts as a 50/50 Beamsplitter. The I-sCMOS - Intensified sCMOS camera records single photons at both outputs of the interferometer. The use of short exposure time of the I-sCMOS, in the single nanosecond timescale, gives it stability and resistance against fluctuations up to tens of MHz..

This mixes the light from both outputs and allows us to observe interference in both outputs of the splitter. The I-sCMOS camera records single photons at both outputs of the interferometer. The use of short exposure time of the I-sCMOS, in the single nanosecond timescale, gives it stability and resistance against fluctuations up to tens of MHz. We collect the data with 200 Hz of frame rate.